Title
Pilot plant demonstration and life cycle assessment of ion exchange processes for CO2 mineralization using industrial waste streams

Author
Christofides, Marios

Publication Date
2023

Peer reviewed|Thesis/dissertation

UNIVERSITY OF CALIFORNIA

Los Angeles

Pilot plant demonstration and life cycle assessment of ion exchange processes for CO_2 mineralization using industrial waste streams

A thesis submitted for partial satisfaction

of the requirements for the degree Master of Science in Chemical Engineering

by

Marios Evangelos Christofides

2023

ABSTRACT OF THE THESIS

Pilot plant demonstration and life cycle assessment of ion exchange processes for CO_2 mineralization using industrial waste streams

by

Marios Evangelos Christofides

Master of Science in Chemical Engineering

University of California, Los Angeles, 2023

Professor Dante A. Simonetti, Chair

A new and attractive technique for reducing emissions by storing carbon dioxide geologically is to capture it within thermodynamically stable, carbonate solids, $CaCO_3$. However, alkalinity is required to achieve favorable conditions for carbonate precipitation (pH >8) from aqueous streams containing dissolved CO_2 (pH <4.5). Utilization of regenerable ion exchange solids have previously been demonstrated to induce alkalinity required for carbonate precipitation from divalent rich brines. In this study, a previously proposed ion exchange process is scaled up to treat 300 L of produced water brine per day for CO_2 mineralization. H^+ saturation capacities were quantified for various inlet concentrations of CO_2 in the gas phase (3 – 20 vol %; 0.10 – 0.81 mmol H^+ per g ion exchange solid) and flow rates (0.5 – 2.0 L min^{-1}; 12 vol %; 0.65 mmol H^+ per g ion exchange solid). Utilizing inlet CO_2 concentration at 0.12 vol %, 0.5 – 3.5 g $CaCO_3$ per L produced

water was precipitated, resulting in energy consumptions ranging from 30 – 65 kWh/t CO_2 sequestered for the ion exchange and mineralization steps. The energy intensity of the process was dependent on volumes ratios of alkaline-rich product and produced water used to precipitate calcium carbonate. Thermodynamic simulations for precipitated calcium carbonate formation were validated through this system, with the primary phases of the precipitated solids in the form of calcite (>97%) with magnesium and iron incorporation from produced water. A life cycle assessment was performed to analyze the net carbon emissions of the technology for two produced water compositions at various inlet CO_2 partial pressures (pCO_2 = 0.03 – 0.20 atm) which indicated a net CO_2 reduction across most conditions studied (0.533 to -0.39 kg CO_2e per kg precipitated calcium carbonate). Emissions were minimized under conditions utilizing concentrated produced waters and CO_2 concentrations greater than 3 vol%. Nano filtration studies showed that the XN-45 membrane can be used to generate a sodium rich permeate stream and a calcium rich retentate stream that can be recycled in the system. The results from this study indicate the ion exchange process can be used to provide alkalinity for the precipitation of carbonate solids for most of the CO_2 concentrations allowing for economic mineralization processes.

The thesis of Marios Evangelos Christofides is approved.

Philippe Sautet

Carlos Morales-Guio

Dante A. Simonetti, Committee Chair

University of California, Los Angeles

2023

Table of Contents

List of figures

Acknowledgments

I would like to thank my parents whose love and support made my academic career possible, as well as my brothers, Dimitrios and Vagelis.

I would like to thank Professor Philip Sautet and Professor Carlos Morales-Guio for agreeing to be members of my committee and for reviewing my thesis.

I would like to thank my advisor, Professor Dante Simonetti, for his guidance and direction, as well as Steven Bustillos, who laid the groundwork for me to follow. His experience with bench and pilot scale studies and valuable feedback on reports and presentations made me a better researcher, and his friendship has been invaluable to me. I would also like to thank the SeaChange and EPOCH groups; I used their labs in Boelter Hall and E6 to perform experiments and supply water to the pilot plant. They are excellent groups with truly great people.

I would also like to acknowledge my childhood friends, Tiam and Sam, with whom I spent a lot of time at UCLA, studying in the basement of the library, walking around the sculpture garden and sitting on the Janus Steps.

1 Introduction

Carbon dioxide (CO_2) is the primary greenhouse gas emitted by human activities[1]. According to the International Energy Agency, global CO_2 emissions from energy combustion and industrial processes reached a new maximum at 36.8 Gt CO_2e in 2022[2], in which approximately 50% of these emissions (18.5 Gt CO_2e) have been generated during the primary energy consumption of oil and gas in the transportation and industrial sectors[3]. The United States contributed approximately 17% (6.3 Gt CO_2e) to total global CO_2 emissions, where approximately 1.4 Gt CO_2e and 1.8 Gt CO_2e were from industrial and transportation sectors[4]. High oil and gas demands consequentially result in large volumes of produced water generated (brine made during the extraction of oil and gas), in which approximately 20 – 25 billion barrels of produced water[5] is generated yearly in the United States leading to increased levels of brine waste and CO_2 emissions (0.5 – 13.5 kg CO_2 equivalent per m^3 produced water processed)[6].

Carbon dioxide mineralization is an attractive strategy that can both limit brine discharge and CO_2 emissions via reacting Ca/Mg-rich brines with CO_2-contanining gaseous streams to produce thermodynamically stable solids in form of calcium or magnesium carbonates[7–9] (e.g., ΔG = -1129.1 kJ/mol for calcite precipitation). Carbon dioxide mineralization approaches avoid separation and storage steps associated with amine-based processes[10,11] and are insensitive to the impurities in CO_2-containing streams (e.g., hydrocarbons, NO_x/SO_x from flue gas[12]). The traditional amine based process has a low CO_2 absorption capacity of approximately 0.35-0.56

mol CO_2/mol Solvent, in addition to the high energy requirement for the regeneration process (3.80 – 4.20 GJ per ton CO_2), due to the high temperatures needed[13].

Due to its reduced process complexity compared to traditional thermal swing amine based processes[14], these processes can be applied under a wide range of operating conditions without substantial modifications and increases in energy requirements to existing plants (e.g., pipeline transportation and monitoring of storage sites).

The utilization of produced water for carbon dioxide mineralization is a viable option due its large range of concentrations for Ca and Mg cations (0.005 M – 0.9 M)[15] and due to the large volume required to treat yearly for safe disposal. However, these streams are typically produced at 4 < pH < 7 requiring a source of alkalinity (e.g., OH^- ions) to drive the formation of carbonate ions (CO_3^{2-}) that induces spontaneous precipitation reactions with divalent cations, as shown in Equation 1:

$$Ca^{2+}(aq) + CO_3^{2-}(aq) \rightarrow CaCO_3\ (s) \quad (1)$$

where the speciation reactions that describe the CO_2–H_2O system are written as:

$$CO_2(g) + H_2O \Leftrightarrow CO_2(aq) + H_2O \Leftrightarrow H_2CO_3(aq) \quad (2)$$

$$H_2CO_3(aq) \Leftrightarrow H^+(aq) + HCO_3^-(aq) \quad (3)$$

$$HCO_3(aq) \Leftrightarrow H^+(aq) + CO_3^{2-}(aq) \quad (4)$$

In water, carbonate anions are the predominant carbon species at pH > 10.3[16], but artificially increasing the pH with caustic soda (e.g., NaOH) would make the mineralization process economically infeasible due to increased energy intensities resulting from caustic soda production (e.g., 1.56 – 2.51 kWh per kg NaOH or 1.1 – 1.8 kg CO_2 per kg NaOH produced depending on the production process[17]).

We have previously demonstrated a regenerable pH swing process (Figure 1)[18,19] based on ion exchange to shift the pH of CO_2-containing aqueous streams from pH 4 to pH > 10, avoiding the need for caustic soda addition. In this ion exchange process, CO_2 from flue gas (pCO_2 = 0.03 – 0.25 atm or pH 4.1 – 4.34) is equilibrated with water to produce an aqueous stream saturated with dissolved inorganic carbon species, as described in equation 2, where dissolved concentrations are dictated by Henry's Law and the thermodynamics of CO_2 speciation in water.[20] Using commercially available ion exchange materials, the reversible exchange of Na^+ and H^+ in solution is described by Equation 5[21,22]:

$$H^+ + R^{Na} \Leftrightarrow R^H + Na^+ \quad (5)$$

where $R^{Na/H}$ is the ion exchange material, present as sodium or proton form and $H^+$and Na^+ are

the ions in solution. As described by Bustillos e. al.[18,19] using weakly acidic cation exchange resin TP-207 (R-1 identifier; Na-form, iminodiacetic acid functional groups), H^+ is removed from the solution while Na^+ is released into solution forming aqueous sodium bicarbonate streams in accordance with Equations 2-5, shifting the equilibrium pH from an initial pH 3.9 to a final pH 11.1, resulting in favorable conditions for carbonate precipitation without the addition of caustic soda. The ion exchange solid can be regenerated using Na-rich brines (e.g., produced water containing 0.05 - 3.0 M Na^+)[15] following depletion of divalent cations that can inhibit Na-exchange capacities due to competitive behaviors.[18,21] The proposed process design is shown in Figure 1 where: (1) acidity is introduced via CO_2 bubbling in deionized water; (2) H^+ - Na^+ exchange using fixed-bed reactors to produce a carbonate-rich effluent stream; (3) carbonate precipitation is induced by mixing with produced water or a Ca/Mg-rich brine; (4) precipitated solids are separated and the remaining effluent is treated via nanofiltration and reverse osmosis for the simultaneous removal of divalent cations and production of a fresh water and Na-rich regeneration stream to be cycled within the process.

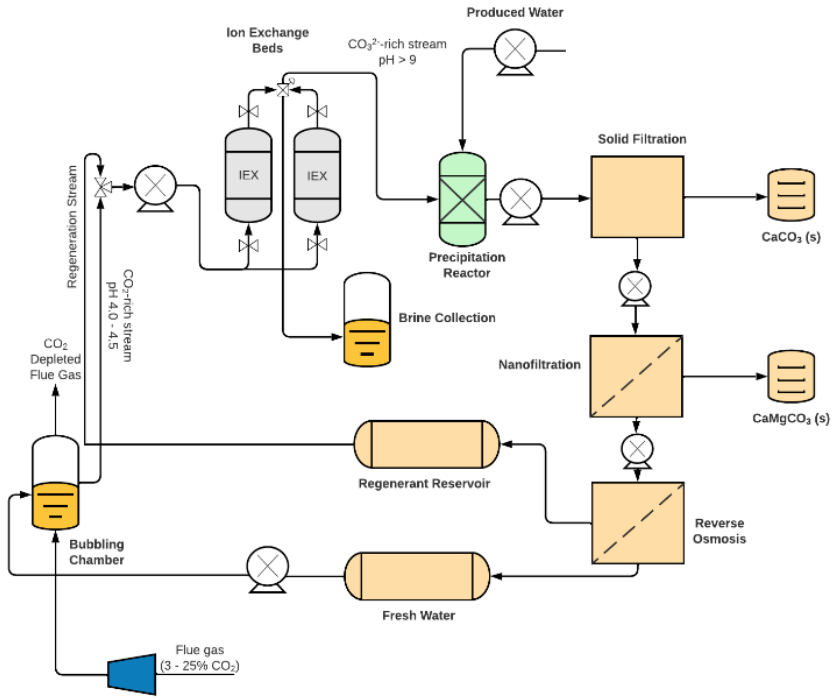

Figure 1. Process flow diagram of the pilot plant scale setup for Carbon Dioxide Mineralization utilizing the Ion Exchange pH Swing

Previous bench-scale experiments and process simulations generated design guidelines of high purity (>97 wt.%) $CaCO_3$ at yields that utilize 3.5 m^3/h of brine from a total bed volume of 0.05 m^3 of regenerable ion exchange material (equivalent to 1 t-CO_2 captured per day).[18,19] In this work, the ion exchange process is scaled up and developed to utilize 300 L of produced water per day (sampled from the Denver-Julesburg Basin and Utica Basin which produce 0.38 billion barrels[5] and 0.61 billion barrels[23] of produced water per day) to sequester 100 – 500 g CO_2 per

day at pCO_2 = 0.03 – 0.20 atm. A life cycle assessment (LCA) methodology is employed to analyze the life cycle or net carbon emissions of the technology. From the results, we identify factors that can potentially swing the results and invalidate our key assumptions through a sensitivity analysis utilizing the experimental pilot plant data.

2 Materials and Methods

2.1 Materials

Sodium chloride (NaCl, >99.0%), sodium hydroxide pellets (NaOH, >98.0%), were all purchased from Fisher Chemicals. 70% nitric acid (HNO_3) and 12.5% hydrochloric acid (HCl) solutions were purchased from Sigma Aldrich. High-purity carbon dioxide (CO_2, 99.99%, Airgas) and high purity nitrogen (N_2, 99.99%, Airgas) were used as a source for the preparation of solutions at varying partial pressures of CO_2. $CaCl_2$ (>93%) and NaCl (>99.0%) All chemicals were used as received unless otherwise stated. Commercially available sodium-form chelating cation exchange resin Lewatit TP-207 (iminodiacetate functional group) was used for the fixed-bed ion exchange experiments. Produced water streams sampled from the Denver-Julesburg Basin (DJ Basin) and Utica (Appalachian) Basin were used for CO_2 mineralization experiments, where compositions of these streams are shown in Table 1. TriSep XN-45 and Suez DK membranes were used for Nanofiltration experiments.

Table 1. Utica and DJW Basin produced water compositions used in this study

Cation	**Utica Basin (mmol/L)**	**DJW Basin (mmol/L)**
Ca	761	6.7
Mg	121	1.9
Fe	1.7	0.4

Na	2495	396

Powder X-Ray diffraction (XRD) patterns of the precipitated phases were obtained on an X-Ray diffractometer (Panalytical X'Pert Pro X-Ray Powder Diffractometer) using Cu Kα radiation of 1.5410 Å to identify the mineral phases of the precipitated solids. Thermogravimetric analysis (TGA) of the precipitated phases was performed on a simultaneous thermal analyzer (STA 6000 Perkin Elmer) to obtain plots showing the mass decomposition precipitate as a function of temperature. Chemical Analysis was performed with an electron dispersion spectrophotometer (EDS; Nova 230 model) with a 10 kV accelerating voltage and a working distance of 5 mm.

2.2 Pilot plant Demonstration for CO_2 mineralization

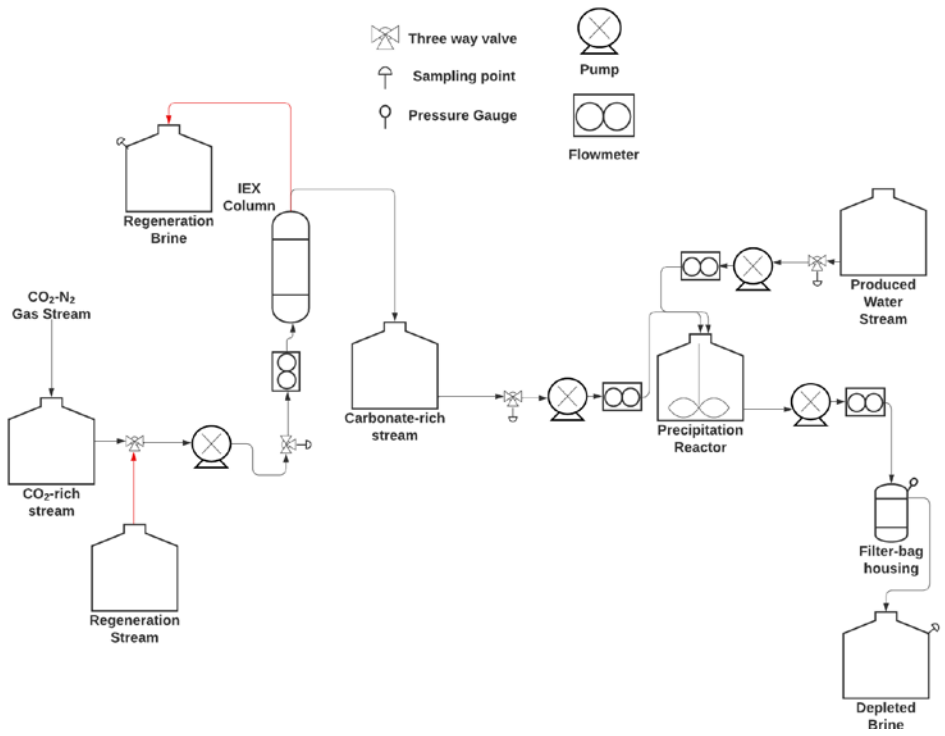

Figure 2. Process flow scheme for the ion exchange demonstration build to utilize 300 L of produced water per day. Carbon Dioxide rich water (pH 4.36,) is directed into the IEX column and collected before being fed into the Precipitation Reactor where it is well mixed with a Produced Water Stream. Precipitated Solids are removed and collected in a Filter Bag Housing Unit.

A 2 L PVC column (3.81 cm diameter, 182.88 cm height) containing TP-207 resin was constructed and held in place by installing mesh size 50 screens at both ends of the column to utilize 300 L of produced water per day for CO_2 mineralization, as shown in Figure 2. Deionized water is bubbled using a gas mixture of N_2 and CO_2 (10 to 50 SLPM) to create an aqueous stream with a CO_2 partial pressure of 0.03 – 0.20 atm (pH 4.25 to pH 4.66 or $[CO_2]$ = 0.001 - 0.0034 M in accordance with Henry's Law; K_H = 30 L atm mol^{-1}). Equilibrium at the desired CO_2 concentration was determined when a stable pH measurement was achieved at the desired pH with respect to Henry's Law. A CO_2-rich stream is fed to a fixed-bed reactor containing ion exchange resin at varying inlet flow rates of 0.5 – 2.0 $Lmin^{-1}$ using a gear pump. The carbonate-rich effluent stream is mixed with a fixed volume of Utica Basin produced water. An overhead mixer is installed in the precipitation tank to ensure turbulent mixing for precipitation (e.g., 750 RPM resulting in Reynolds Number = 49,302). The slurry containing precipitated $CaCO_3$ is then fed through a filter bag housing (solid separator; 3 µm filter bags) where the precipitated $CaCO_3$ is filtered from the solution. A synthetic regenerate stream in accordance with effluent compositions obtained from thermodynamic simulations (~0.5 M NaCl; pH 9 – 11 dependent on volume ratio used) was used to regenerate the ion exchange column.

A standard cross flow cell was used for Nano filtration experiments. The cell area was 0.42 cm^2 and operated at a max pressure of 80 psi. A cooling system was installed to maintain the temperature of the feed solution, to counteract the heat generated by the pump. The temperature of the feed was kept at 25 °C.

2.2.1 Fixed-bed ion exchange experiments for dynamic capacities

Flow-rate studies using pCO_2 = 0.12 atm were performed at 0.5, 1.0 and 2.0 L min^{-1} until the effluent pH (or H^+ concentration) was equivalent to that of the inlet. Effluent samples were collected every 5 minutes in the first hour and every 10 minutes in the time after. The developed breakthrough curves are presented as the normalized effluent H^+ concentration (Equation 6) as a function of the number of normalized bed volumes (NBV; Equation 7).

$$\text{Normalized Effluent Concentration} = \frac{C_{effluent}}{C_{inlet}} \quad (6)$$

$$\text{Normalized Bed Volume} = \frac{Q*t}{BV} \quad (7)$$

where Q is the liquid flowrate (L min^{-1}), t is the time (min), NBV is the number of bed volumes processes (L). Similarly, the effect of inlet CO_2 concentrations on the H^+ exchange capacities were performed using the following inlet CO_2 concentrations: 1.0 atm/pH 3.9, 0.5 atm/pH 4.1, 0.25 atm/pH 4.2, and 0.12 atm/pH4.36. The fixed-bed H^+ exchange capacities (CEC_H) are quantified using the following equation:

$$CEC_H = \frac{[H]_{in} - [H]_{out}}{m} \quad (8)$$

where $[H]_{in}$ is the total moles of H^+ fed into the reactor and $[H]_{out}$ is the total moles of H^+ out of the reactor, quantified by calculating the area under the breakthrough curve using the trapezoidal rule.

2.2.2 Fixed-bed ion exchange experiments cycling experiments for CO_2 mineralization

Cycling of the ion exchange process to utilize 300 L of produced water per day was performed using inlet pCO_2 = 0.12 atm (pH 4.34) at a fixed inlet flow rate = 1.0 L min^{-1} until a breakthrough pH 9.5 was attained. Regeneration of the ion exchange reactor was performed using background 0.5 M NaCl concentrations at pH 9, pH 10, and pH 11. The ion exchange resin was cycled 9 times to successfully utilize 300 L of produced water in 24 hours of operation.

CO_2 mineralization experiments were performed using effluent collected from the breakthrough ion exchange cycling experiments using Utica produced water. The carbonate-rich effluent from the ion exchange reactor was mixed with the produced water at varying volume ratios in the precipitation tank according to the following volume ratio (V_R) equation: The effluent was then collected, and vacuum filtered to recover the solid. It was then dried at 60 ℃ for 24 hours in a laboratory oven. Volume ratios V_R, were defined as

$$V_R = \frac{V_{PW}}{V_{PW}+V_{IEX}} \quad (9)$$

where V_{IEX} is the volume of IEX solution from the effluent of the column and V_{PW} is the volume of produced water. The IEX solution and produced water were stirred for one hour to maximize calcium carbonate precipitation. The slurry was then fed into a filter bag housing unit separate the solids. The collected solids were then dried at 60°C for 24 hours and the effluent solution concentrations were analyzed via inductively coupled plasma – optical emission spectroscopy (ICP-OES; Avio 200 ICP Optical Emission Spectrometer, Perkin Elmer). Samples were filtered

through a 0.2 micron corning filter and diluted in 5% (w/w) HNO_3 (prepared by diluting 70% HNO_3 in ultra-pure water). The solids were further analyzed via powder x-ray diffraction and SEM/EDS as previously described.

2.3 Thermodynamic modeling of precipitation products

The activities and speciation of aqueous components were calculated using GEMSelektor, version 3.4, which includes a native GEM (Gibbs energy minimization) solver,[24,25] a built-in NAGRA-PSI 'Kernel', and the slop98.dat and Cemdata18 thermodynamic databases.[26–29] Thermodynamic data for the solid phases are shown in Table S1, and thermodynamic data for aqueous species/complexes and gases are shown in Tables S2 and S3, respectively. Thermodynamic data for nesquehonite ($MgCO_3.3H_2O$),[30] hydromagnesite ($Mg_5(CO_3)_4(OH)_2{\cdot}4H_2O$) [31], dolomite ($(Ca_{0.5}Mg_{0.5})CO_3$),[31] monohydrocalcite ($CaCO_3.H_2O$),[30] and an iron-calcium carbonate solid-solution model ($(Ca,Fe)CO_3$)[32] were included in the simulations. Thermodynamic data for metastable nesquehonite and hydromagnesite were included as potential magnesium carbonate phases, opposed to 'natural' mineral thermodynamic data to represent the short-term precipitation time. The dolomite phase was chosen to represent partial calcium replacement by magnesium within $CaCO_3$. The $(Ca,Fe)CO_3$ non-ideal solution model was developed in a CaO-MgO-FeOOH-CO_2 system to represent iron (II) replacement within the $CaCO_3$ structure in the presence of magnesium.[32]

The activity of any relevant ion species is described within GEMS using the Truesdell-Jones modification of the extended Debye-Hückel equation that is applicable for ionic strengths (I,

mol/L) less than 2 mol/L (see Equation 10)[33]:

$$\log \gamma_i = \frac{-Az_i^2\sqrt{I}}{1 + \dot{a}B\sqrt{I}} + b_\gamma I + \log \frac{X_{jw}}{X_w} \quad (10)$$

where, γ_i and z_i are the activity coefficient and charge of the i^{th} aqueous species respectively, A and B are temperature- and pressure-dependent coefficients, I is the molar ionic strength, X_{jw} is the molar quantity of water, and X_w is the total molar amount of the aqueous phase. A common ion size parameter, ȧ (3.72 Å) and short-range interaction parameter, b_γ (0.064 kg·mol^{-1}), are used as constants for the NaCl background electrolyte.[33] NaCl was selected as the dominant electrolyte throughout this study to simulate the IEX product solution compositions and pH because of constantly larger NaCl concentration in solution. Solution compositions in the simulations used the V_R ratios as described by Equation 9 and the concentrations of produced waters described in Table 1.

2.4 Energy intensity of the pilot plant for CO_2 mineralization

Energy calculations were performed on the process, to account for mixing, pumping, and solid separation from the process and to show the impact this process can have on CO_2 sequestration and utilization.

The hydraulic power used by the pump was found from equation 11[34]

$$P_h = q * h * \frac{\rho}{367} \quad (11)$$

where q is the flow rate, g is the acceleration of gravity, h is the differential head, and ρ is the density of the liquid.

The shaft power used by the pump was found from equation 12[34]

$$P_s = P_h/\eta \quad (12)$$

where P_s is the shaft power, P_h is the hydraulic power and η is the pump efficiency. The power associated with the mixer was calculated using the following equation.[35]

$$P_m = N_p * n^3 * d^5 * g * Re \quad (13)$$

where $P_m$is the mixing power, $N_p$is the impeller power number, n is the impeller rotational speed, d is the impeller diameter, g is the specific gravity of the fluid and Re is the Reynolds number of the system.

2.5 Life cycle assessment

2.5.1 Goal

A life cycle assessment (LCA) was conducted in this study based on ISO 14040[36] and ISO 14044[37]. The function of the product system was to produce precipitated calcium carbonate via an ion exchange process in the United States in different scenarios and the reference flow of the functional unit (FU) was 1.0 kg of precipitated calcium carbonate, which is an established measurement basis in the scientific and technical literature[38,39]. The modeling approach adopted

was the attributional LCA and the product system extended from cradle to precipitated calcium carbonate plant gate, because the use and end-of-use of processes for the product will not differ for the manufacturing technologies. The main goal of this study is to investigate the environmental life cycle impacts of calcium carbonate precipitation recovered from utilizing produced water streams. Yield data from utilizing 300 L of produced water per day is scaled up in the geographical context of the United States (e.g., different regions/sources of produced water from the Utica and Colorado Basins, different grid-electricity sources for the process, and varying pCO_2) to determine the impacts of different produced water streams.

2.5.2 Boundary

The system boundaries span from raw material procurement to the actual precipitated calcium carbonate manufacturing process as shown in Figure 3. For traditional precipitated calcium carbonate production, the boundary includes limestone mining, while in the case of the ion exchange system the solid raw materials are considered to be a waste stream that would be formed, whether or not utilized in precipitated calcium carbonate manufacturing. The system boundary for the precipitation of calcium carbonate in Figure 3 adopts a “cradle-to-gate” approach in which it only includes raw material acquisition and manufacturing processes and excludes transportation to distribution site, use and end-of-life (EOL) stages. Thus, the ion exchange system boundary is not extended to steelmaking processes or to limestone mining, but instead it considers the avoided waste material streams (CO_2 and produced water/brine).

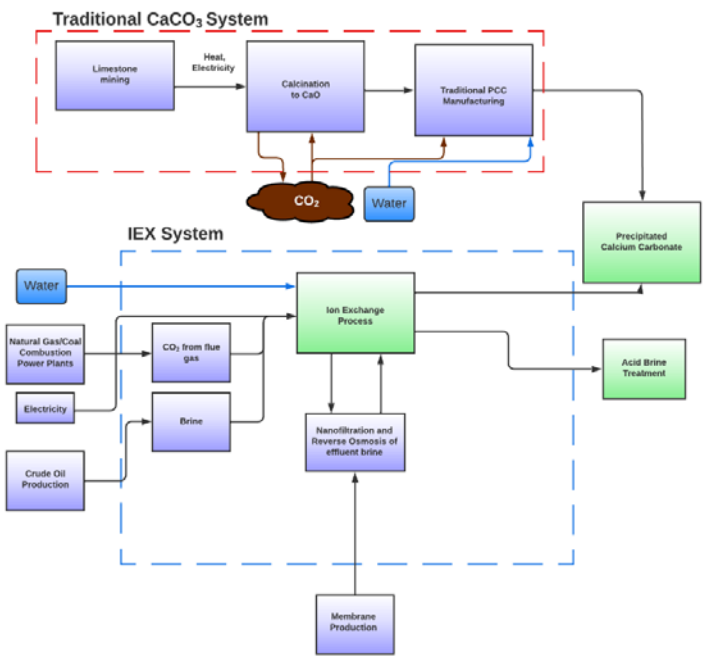

Figure 3. System boundaries (dashed lines) for traditional precipitated calcium carbonate production (red) and for precipitated calcium carbonate production via the ion exchange process (red).

Additionally, emissions from the manufacturing of the ion exchange solid used is not considered due to its extensive regeneration capacity (>99%) as discussed in this study. The system is extended to include membrane filtration treatment steps of the process for the cycling of the ion

exchange process (Figure 1) at appropriate water recovery ratios. Make-up water is added back into the system to account for water losses from the effluent treatment steps.

2.5.3 Allocation and scenarios description

This study investigates the pilot-scale production of precipitated calcium carbonate using the best and worst-case scenarios of the process, defined by varying energy-intensive processes, such as the processing of deionized water and effluent brine for cycling the process for the two produced waters investigated in this study. The scenarios to produce 1 kg precipitated calcium carbonate are described in Table 2.

Table 2. Summary of the main parameters used in the assessed scenarios for the production of 1 kg precipitated calcium carbonate

Item	S1	S2	S3	S4	S5	S6	S7	S8	S9
Input									
Carbon Source	3%	12%	20%	12%	12%	12%	12%	12%	12%
Produced water	Utica Basin	Utica Basin	Utica Basin	DJ Basin	Utica	Utica	Utica	Utica	Utica
Electricity	Average USA	Average USA	Average USA	Average USA	US Average Coal	US Average Natural Gas	US Average Renewable	Average USA Easter	Average Western USA
Output									

Dilute Acidic Brine	No utilization (100%)	No utilization (100%)	No utilization (100%)	No utilization (100%)	No utilization (100%)	No utilization (100%)	No utilization (100%)	No utilization (100%)	No utilization (100%)

Nine scenarios for production of calcium carbonate via the ion exchange process were assessed as follows:

- S1 – S3 describe the utilization of CO_2 from flue gas at 3 – 20 vol% CO_2 utilizing the Utica Basin produced water and the average electricity input for the United States
- S4 describes the utilization of CO_2 from flue gas at 12 vol% CO_2 utilizing the DJ Basin produced water and the average electricity input for the United States
- S5 – S9 describe the utilization of CO_2 from flue gas at 12 vol% CO_2 utilizing the Utica Basin and various sources of electricity inputs for the United States

For each scenario, calculated electricity inputs from the pilot plant were input for the precipitation of calcium carbonate (e.g., pumping, agitation). A deionized water recovery of 88% is calculated based on traditional nanofiltration and reverse osmosis water recovery rates for brines of similar compositions following mineralization[40,41]. Makeup deionized water is fed back into the system to account for water-reductions from generation of regeneration streams.

2.5.4 Life cycle inventory

The life cycle inventory (LCI) was collected using different sources of data provided in the following sections. LCI was mainly obtained from the ecoinvent v3.8 database using the cut-off allocation library found in SimaPro 9.1 software.

2.5.5 Life cycle impact assessment

This LCA study uses the updated ReCiPe 2016 midpoint (H) method available in SimaPro 9.1 software to compare the ion exchange process to the traditional precipitated calcium carbonate process. The midpoint method consists of 18 environmental indicators, including global warming, fine particulate matter formation, human carcinogenic toxicity, water consumption, etc. The ReCiPe method is used in this study as it is based on the global average data. Contribution analysis is performed for the precipitated calcium carbonate to identify the hotspots only using the global warming indicator. The comparisons between precipitate calcium carbonate production processes is performed using the ReCiPe global warming indicator, which is calculated based on the Global Warming Potential (GWP) IPCC 2007 indicator for a time frame of 100 years.

3 Results and Discussion

3.1 Pilot Plant Demonstration for CO_2 mineralization

3.1.1 Fixed-bed ion exchange experiments for dynamic capacities

Flow rate is a key parameter to evaluate the efficiency of ion exchange materials in a continuous process because contact time and column hydrodynamics (e.g., Reynolds number) can impact ion exchange capacities[42–45]. Flow rate studies were conducted on a pilot plant to determine H^+ saturation capacities using a 2 L bed volume and organic cation exchange resin TP-207 (R-1) at fixed inlet partial pressures of CO_2. The effect of inlet flow rates (0.5 L min^{-1}, 1.0 L min^{-1} and 2.0 L min^{-1}; Re 16.4, 32.8, 65.6 respectively) and inlet CO_2 concentrations at fixed flow rate on H^+ saturation capacity were found using carbon dioxide concentrations similar-to flue gas (e.g., pCO_2 = 0.03 – 0.20 atm), shown in Figure 4.

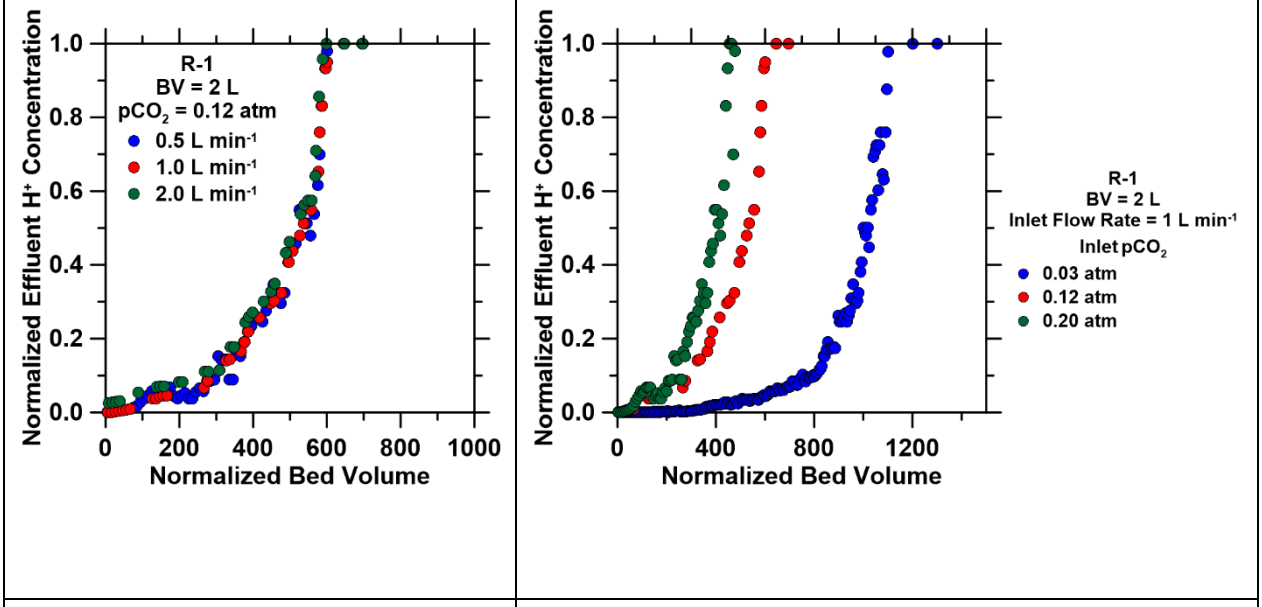

(a) **(b)**

Figure 4. Breakthrough curves for the H^+ exchange reactions for **(a)** inlet pCO_2 = 0.12 atm at varying inlet flow rates and **(b)** inlet pCO_2 = 0.03 – 0.12 atm at fixed flow rate 1 L min^{-1} as a function of normalized bed volume.

Saturation H^+ capacities (quantified when the outlet H^+ concentration was equivalent to 95% of the inlet H^+ concentration) of the ion exchange resin were unaffected by changes to inlet flow rates (e.g., no change in breakthrough curve shown in Figure 3a at different flow rates), resulting in 0.65 mmol H^+ per g ion exchange solid and in range of H^+ uptake capacities measured at the bench scale (e.g., 0.60 – 0.90 mmol H^+ per g ion exchange solid[18]). Furthermore, H^+ uptake

capacities were quantified at varying inlet pCO_2 (Figure 3b; Table 3) to similarly confirm previous bench-scale performance at higher inlet flow rates and scale.

Table 3. H^+ saturation capacities are varying inlet pCO_2 at fixed inlet flow rate 1 L min^{-1}

Pco_2 (atm)	**Uptake Capacity (mmol H^+ per g)**
0.03	0.10
0.12	0.65
0.20	0.91

As shown in Table 3 and previously shown at a lower scale[18], H^+ uptake capacities increase with higher initial CO_2 concentrations, ranging from 0.10 to 0.91 mmol H^+ per g ion exchange resin. The driving force for ion exchange is the concentration difference between the solute on the sorbent and the solute in solution[18,21,46], resulting in shorter breakthrough times (e.g., rapid filling of binding sites with H^+ in solution) and larger capacities for smaller inlet CO_2 concentrations. Increased pCO_2 levels in the inlet stream result in increased H^+ concentrations as described in equation 2, resulting in increased saturation capacities. Significantly, measured saturation capacities across varying inlet CO_2 concentrations are consistent with those previously measured at the bench-scale[18], indicating successful scale-up and performance of the ion exchange resin.

3.1.2 Fixed-bed ion exchange experiments for CO_2 mineralization

To determine the feasibility of ion exchange solids for regenerative use in a continuous process, experiments were performed over a 24-hour period utilizing 300 liters of Produced Water to precipitate calcium carbonate solids. Deionized water was equilibrated with carbon dioxide, 0.12 atm (pH 4.36), and subsequently fed to the ion exchange column with an inlet flow rate of 1 L min^{-1}. The column operates until the effluent pH reaches pH 9 to achieve alkaline conditions needed for calcite precipitation. The carbonate-rich effluent is then contacted with the Utica produced water streams for $CaCO_3$ precipitation. The pH swing process is shown across 9 cycles in Figure 4a. An initial pH of 4.36 increases to a maximum of pH 11.8 after in contact with the ion exchange resin. Following breakthrough based on the effluent pH, cycling of the ion exchange solid was performed via regeneration of the ion exchange resin was performed using pH 9,10,11, and 12 (e.g., effluent pH following $CaCO_3$ precipitation[18,19]), shown in Figures 5b for 9 cycles (amount required to utilize the desired volume of produced water).

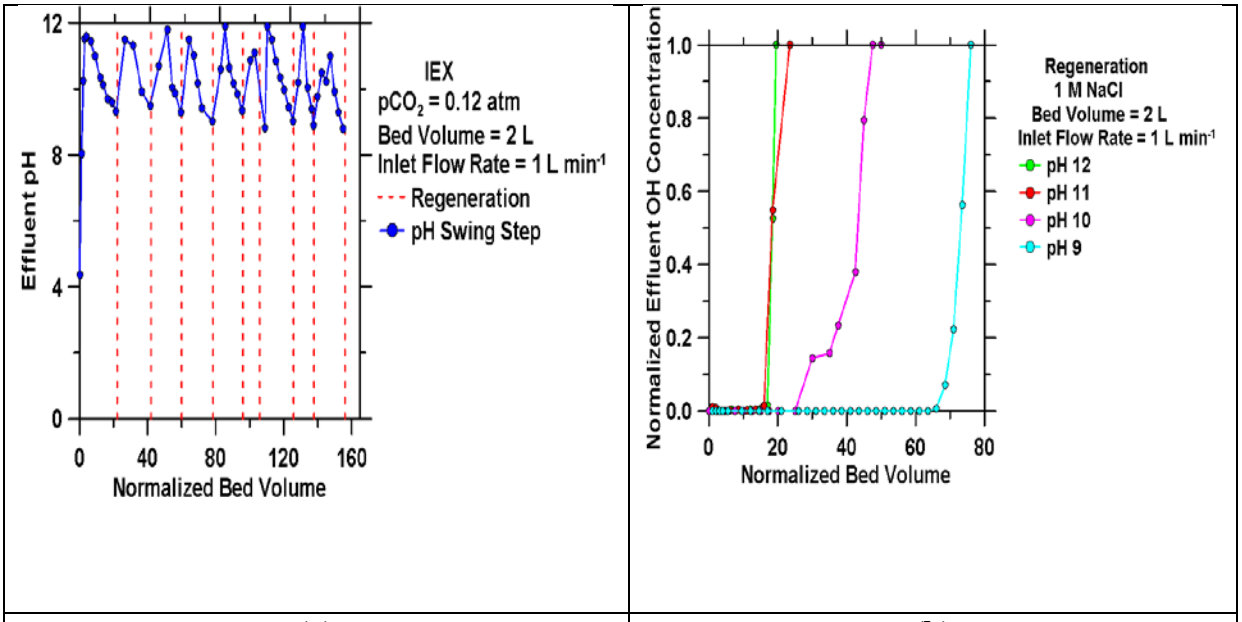

(a) **(b)**

Figure 5. **(a)** effluent pH as a function of normalized bed volume for cycling of the ion exchange solid at 1.0 $Lmin^{-1}$and an inlet pCO_2 = 0.12 atm and **(b)** normalized effluent hydroxide concentration as a function of normalized bed volume at inlet pH 9, 10, 11 and 12 using background 1 M NaCl.

The breakthrough time and regeneration of the ion exchange resin was consistent across multiple cycles at the same flow rates and initial carbon dioxide feed. This is expected as the residence time between the carbonate rich feed solution and the ion exchange resin was consistent across multiple cycles. The proton removal performance of the resin did not diminish over time as a maximum pH > 10 was achieved within each cycle following regeneration. As previously

discussed in Lee 2016, resin capacities as a function of pH can change[47] (e.g., regeneration pH larger than the pKa of the ion exchange functional group to deprotonate ion exchange sites). Regenerating at different pH confirms the relationship between alkalinity and regeneration time, as the pH following mineralization can vary due to the concentration of ions in solution. The normalized bed volume required for regeneration increases with decreasing hydroxide concentrations (decreases in regeneration pH) as seen in Figure 5b. More alkaline solutions result in faster regeneration times due to the larger concentration gradient in hydroxide ions that remove protons from the ion exchange resin. These results are significant as larger regeneration time requirements would result in increased energy intensities associated with pumping energies.

3.1.3 CO_2 mineralization using produced water streams

To quantify the volume requirement (e.g., volume of carbonate-rich stream to produced water stream) needed to maximize $CaCO_3$ precipitation (and CO_2 sequestration) in the process, thermodynamic simulations were performed at varying volume ratios and CO_2 concentrations for Utica and DJ Basin produced water samples, shown in Figure 6**.**

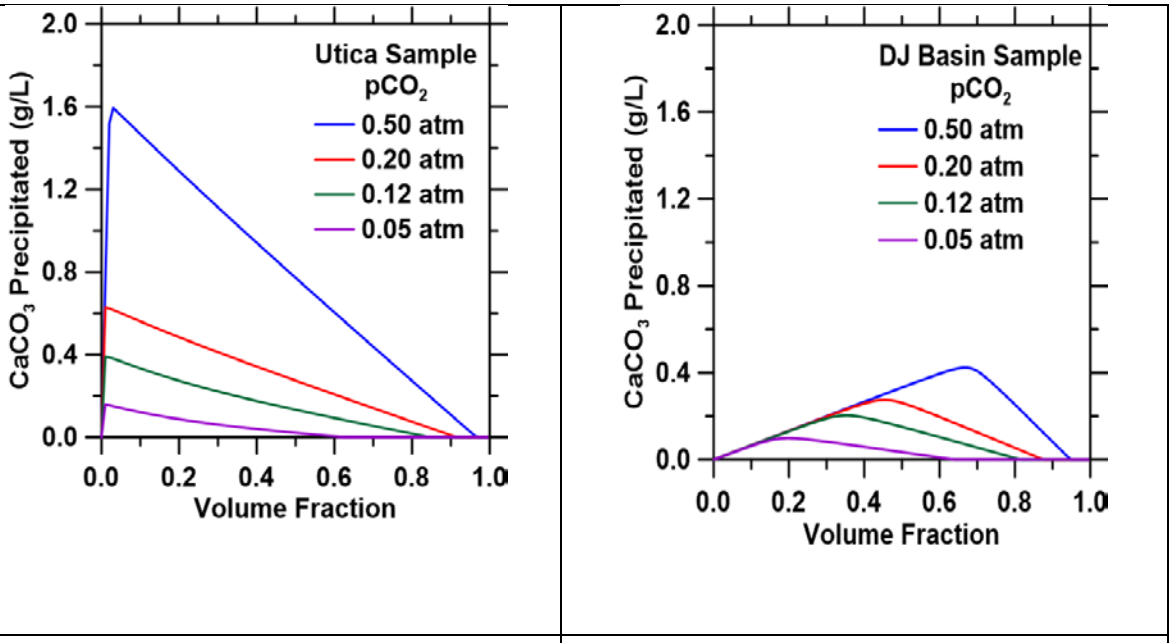

(a) **(b)**

Figure 6. Calcium carbonate precipitation as a function of volume fraction for **(a)** Utica and **(b)** DJ Basin produced water streams.

As shown in Figure 6, significant differences in maximum precipitated $CaCO_3$ yields between the two produced water streams are a result of the larger differences between initial calcium concentrations (Table 1). Calcium carbonate yields increase with larger CO_2 concentrations for both produced water streams, ranging from 0.18 – 1.6 g $CaCO_3$ per L of total solution for Utica produced water and 0.16 – 0.60 g $CaCO_3$ per L of total. As previously discussed, calcium carbonate yield changes with changing volume ratios and is maximized when the [Ca]:[CO_2] ratios in solution are 1:1[18,19]. Different ratios of produced water have different concentrations of calcium, changing how much calcium carbonate can be precipitated from the system. Lower

volumes of produced water used would require the system to generate more ion exchange effluent to reach the same volume target of 1 Liter, increasing the energy intensity of the system. To study the viability of ion exchange resin using higher volumes of solution, pilot plant studies were conducted to utilize 300 Liters of Utica produced water, shown in Figure 7.

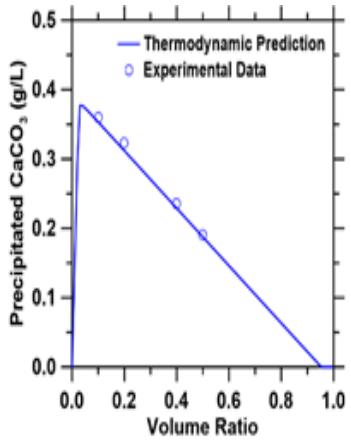

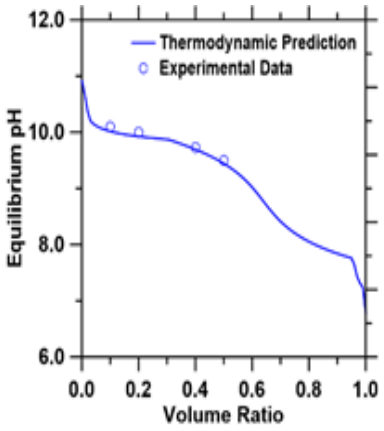

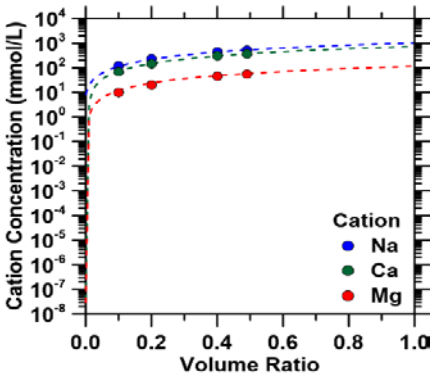

(a)	(b)	(c)

Figure 7. a) Thermodynamic simulations and experimental data displaying precipitated $CaCO_3$ yields as a function of volume ratio (produced water to the total volume of solution) at pCO_2 = 0.12 atm using the described produced water composition above. **b)** Thermodynamic simulations and experimental data displaying pH as a function of volume ratio (produced water to the total volume of solution) at pCO_2 = 0.12 atm using the described produced water composition above **c)** Cation Concentration of Na, Ca and Mg as a function of volume ratio following mineralization.

Predicted and experimental yields for calcium carbonate precipitation as a function of volume ratio are shown in Figure 7a. Precipitated calcium carbonate yields are maximized at smaller volume ratios (e.g., larger volumes of carbonate-rich solution) at 0.36 grams of calcium carbonate

per liter of solution and decreases to 0.21 g $CaCO_3$ per L of solution at a 0.5 volume ratio. The experimental mass of precipitated calcium carbonate, pH and cation concentrations agree with the thermodynamic simulation data, additionally showing these predictions can be applied to different compositions of brines. Furthermore, validation of pH and cation concentrations (Figure 7b-c) following mineralization is important as these concentrations will affect downstream treatment of the effluent to cycle the process (e.g., nanofiltration and reverse osmosis steps). A regeneration stream at a higher pH will result in faster regeneration times compared to lower pH streams (Figure 5b). Additional separation of residual calcium and magnesium ions will affect the energy intensities of the membrane filtration steps (e.g., larger concentrations at higher volume ratios will increase osmotic pressures and in turn operating pressure requirements). The concentration of ions in solution will have an impact on the energy requirement of the nanofiltration step. These energy requirements have previously been quantified for effluent streams containing 50 – 300 mmol/L Na, similar to those measured in this pilot plant, where energy for membrane filtration of this stream results in up to 0.50 MWh/t of CO_2 sequestered to the process[19].

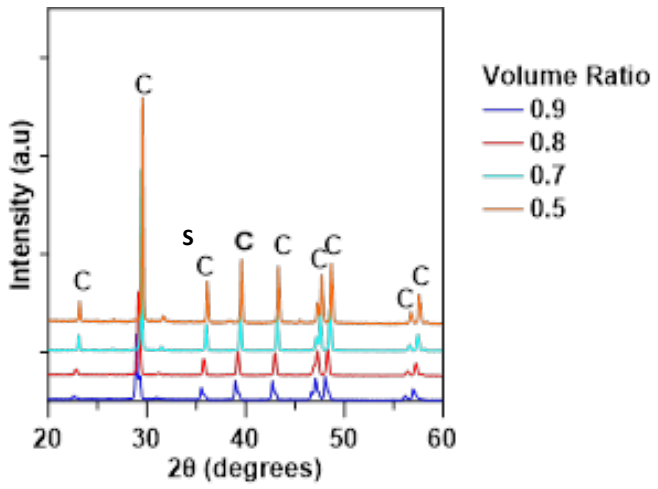

(a)

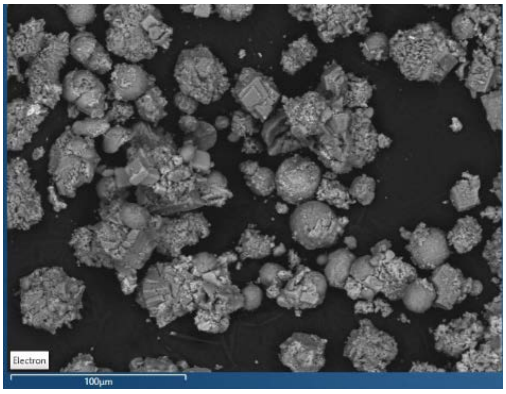

(b)

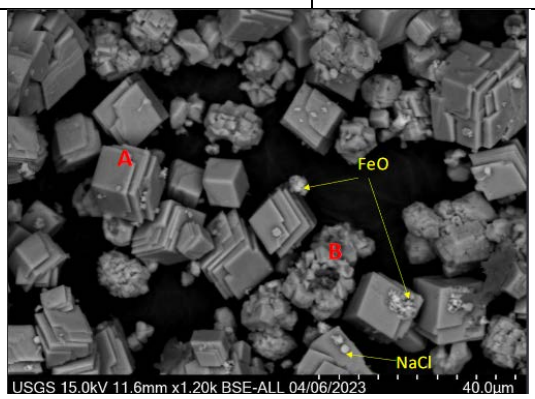

(c)

Figure 8. a) X-ray diffraction patterns for precipitated calcium carbonate solid at volume ratios of 0.5, 0.7, 0.8, and 0.9 Utica produced Water to IEX solution and SEM images of precipitated

solids at volume ratios of **(b)** 0.5 and **(c)** 0.9.

Precipitated calcium carbonate solids were analyzed for phase formations and morphologies as shown in Figure 8. X-ray diffraction patterns (Figure 8a) for four solid samples collected from volume ratios 0.9 to 0.5 show calcite (labeled "C") as the primary phase in for each volume ratio with small presence of siderite (iron (II) carbonate; labeled S)[48]. Significant diffraction peak shifts are observed as volume ratio is decreased (e.g., increases in volume of produced water used for mineralization). This is likely a result of divalent cation incorporation into the $CaCO_3$ structure (e.g., potential Mg, Sr, Fe incorporation into calcite structures[49–52]). As shown in Figure 8 b-c, significant changes in calcite morphology are observed when decreasing volume ratios. At a large volume ratio, the conventional rhombohedral structure for calcite is observed with small amounts of spherical solids (identified as FeO via EDS) which are likely siderite phases.[53] When decreasing volume ratios (increasing produced water content), the morphology of crystals change significantly to spherical structures, with no FeO detected. These changes in morphology are likely a result of Mg or Sr incorporation as these ions change the morphology of calcite from rhombohedral to either elongated needle-like structures or spheres (representative of amorphous calcium carbonate)[49,52]. Acid digestion of the precipitated solids at volume ratios 0.5, 0.8 and 0.9 were performed to confirm possible cation incorporation (Figure S1). As shown in Figure S1, as volume ratio decreases (increasing produced water content) the concentrations of magnesium and iron dissolved from the solids increase significantly, indicating cation incorporation. Furthermore,

thermogravimetric analysis was performed (Figure S2) and confirmed >97% $CaCO_3$ for the precipitate solids.

3.1.4 Energy intensity of the ion exchange pilot plant

The energy requirements of the pilot plant were quantified for different volume ratios of produced water and ion exchange effluent. Intensities were calculated for the pilot operating at a flow rate of 1 L min^{-1} with one hour of mixing. The energy intensities are shown in Figure 9 as a function of volume ratio, normalized by mass of CO_2 sequestered in solid form.

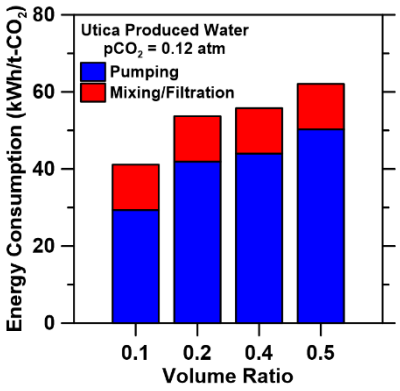

Figure 9. Energy Intensity of the ion exchange pilot plant for CO_2 mineralization as a function of volume ratios.

As shown in Figure 9, energy consumption for the pilot plant increases from 40 – 62 kWh per ton CO_2 sequestered as volume ratio increases because of decreased $CaCO_3$ yields resulting in larger volume requirements. Pumping energy requirements contribute to >70% of the energy intensities, ranging from 29.3 – 50.3 kWh per ton CO_2 sequestered where ass filtration and mixing contributes 9.1 – 11.8 kWh per ton CO_2 sequestered. Previous process simulations estimated an energy intensity range of 40 - 95 kWh/t-CO_2 for ion exchange pumping and solid separation steps for various produced water compositions and volume ratios[19], placing these energy intensities in the range of previous predictions and validating previous process simulations. In combination with thermodynamic simulations to predict yields, process simulations can be performed to predict the energy intensities of the ion exchange steps. Utilizing volume ratios that maximize precipitated calcium carbon (and CO_2 sequestration) is essential to minimizing energy requirements from the alkalization and precipitation steps of the process These energy intensities and measured yields are used to develop a life cycle assessment for the ion exchange process. Further process simulation validation may be needed to validate the energy intensities from the membrane filtration treatment steps.

3.1.5 Life cycle assessment of the ion exchange pilot plant

A life cycle assessment method was performed to quantify net carbon emissions of the ion exchange technology for CO_2 mineralization for various scenarios detailed in Table 2 to produce 1 kg precipitated calcium carbonate. Table S4 provides the life cycle assessment inputs, databases used, and results for the precipitation of calcium carbonate via ion exchange. The global warming

potential for various scenarios and the different steps of the ion exchange process is shown in Figure 9. Mass of CO_2 sequestered and energy intensities from the ion exchange pilot plant were used to as inputs for the various scenarios. To extend the analysis for the entire process, previously quantified nanofiltration and reverse osmosis energy intensities[19] were used and make-up deionized water is added back into the system for complete cycling of the process to produce 1 kg precipitated calcium carbonate, detailed in Section 2.5.3.

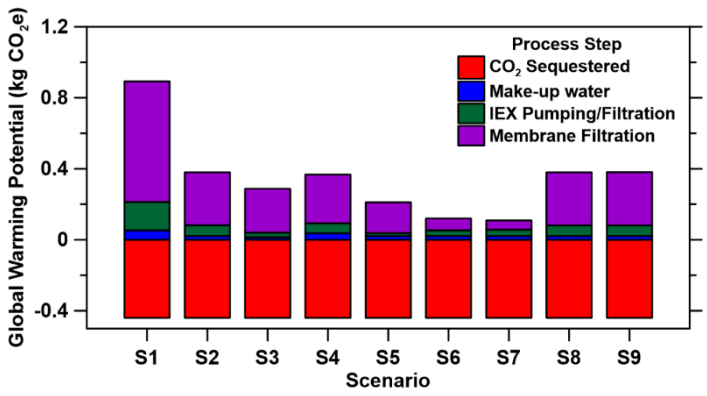

(a)

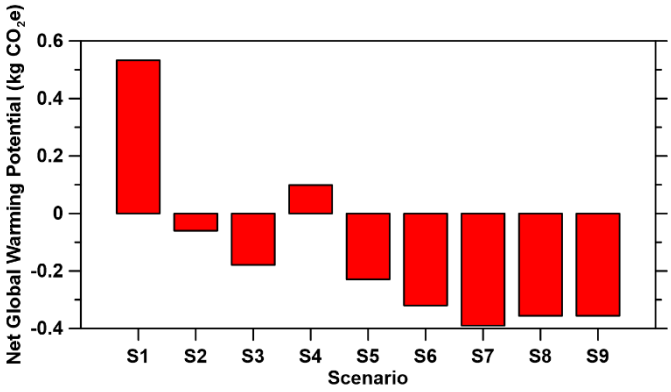

(b)

Figure 10. (a) Global warming potential and **(b)** net global warming potentials to produce 1 kg precipitated calcium carbonate for various scenarios.

Scenarios 1 – 3 detail the global warming potential for the utilization of Utica Basin produced water at pCO_2 = 0.03 atm, 0.12 atm and 0.20 atm, respectively, using the average United States electricity intensity[3]. Increasing inlet concentrations of CO_2 results in water requirement reductions and energy pumping requirements to produce 1 kg precipitated calcium carbonate. As shown in Figure 9b, Scenario 1 has in the highest net global warming potential at 0.533 kg CO_2e per kg precipitated calcium carbonate compared to scenarios 2 and 3 (-0.06 kg and -0.179 kg per kg precipitated calcium carbonate) due to the larger energy requirements from membrane filtration (1.8 kWh/kg precipitated calcium carbonate compared to 0.6 kWh/kg precipitated calcium carbonate) with ion exchange processing only contributing 0.09 kg CO_2e to total emissions in this scenario. Scenario 4, which utilizes a more dilute produced water (DJ Basin) at pCO_2 = 0.12 atm, results in a net positive global warming potential at 0.10 kg CO_2e per kg precipitated calcium carbonate because of inherently smaller initial calcium concentrations that result in smaller calcium carbonate yields compared to using more concentrated produce water. Despite positive net emissions in scenarios 1 and 4, these emissions are comparable to traditional precipitated calcium carbonate processes which emit between 0.35 – 1.04 kg CO_2e per kg precipitated calcium carbonate produced[38].

A sensitivity analysis was performed to account for the different locations produced water can be sourced and different sources of electricity that can power the process (Table 2; electricity from natural gas, coal, renewables; average electricity grid comparing Eastern and Western United

States). Scenarios 5 – 7 show the global warming potentials utilizing Utica produced water and the United States emissions average electricity for using coal, natural gas and renewable sources (e.g., wind turbines)[3,54], respectively, using pCO_2 = 0.12 atm (representative of flue gas). Net global warming potentials are negative for each scenario, minimized by using renewable energy at -0.39 kg CO_2e per kg precipitated calcium carbonate. Small changes in net emissions are observed when utilizing the average electricity grid from western and eastern United States[2,54] resulting in -0.356 kg CO_2e per kg precipitated calcium carbonate produced. Significantly, these results show the impact initial brine compositions and CO_2 concentrations have on the net emissions of the process. Net emissions are significantly reduced using more concentrated streams of brine and CO_2. The overall process would require optimization for more dilute brines and CO_2 streams to maximize yields and minimize energy intensities.

3.1.6 Separation of Ions via Nanofiltration

Once the column effluent and produced water solution have been well mixed and filtered to precipitate and recover calcium carbonate solids, the solution would be treated via nanofiltration to recover calcium rich retentate and sodium rich permeate streams that could be recycled back into the system. Synthetic solutions were made based on Ca and Na concentrations in the post solid recovery solution. The first membrane studied, XN-45, was chosen due to the high rejection of magnesium and calcium in comparison to sodium[55]. The Suez DK membrane was chosen due to the low rejection of sodium chloride[56]. Experiments were performed using a 10 mmol/L $CaCl_2$ and 10 mmol/L NaCl –$CaCl_2$ using a cross flow cell. The sodium rejection performance is shown in Figure 11 for the Suez DK membranes. An ideal sodium rejection would be less than 10%, with experiments achieving a rejection of less than 30%. The membrane has potential for the IEX process but is not ideal.

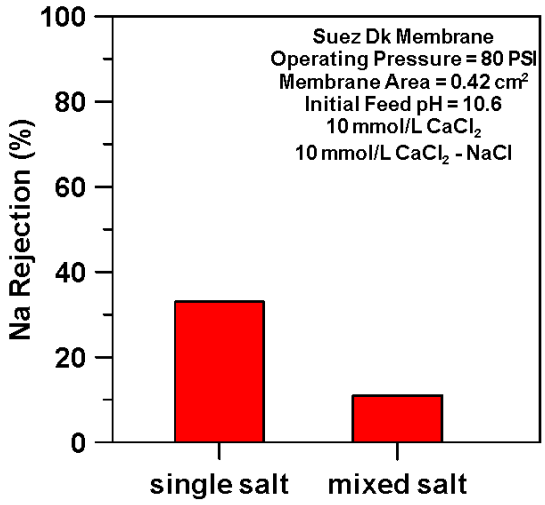

Figure 11. Sodium rejection for single and mixed salt using Suez DK membrane.

The sodium rejection of the Suez DK membrane is not ideal for the purposes of the Ion Exchange Process. The rejection of the single salt was greater than 30% and for the mixed salt was better at 12%, as shown in Figure 11. The purpose of creating a sodium rich permeate stream is to use it for the regeneration of the Ion Exchange resin, reducing the need for foreign stoichiometric agents in the process. The calcium rejection will be an important parameter in determining the feasibility of this membrane. Calcium rejection of the XN-45 and Suez DK Membranes was tested using a synthetic calcium chloride solution and was able to achieve an ideal rejection of 99% with a sodium rejection less than 10%. The purpose of creating a calcium rich retentate

stream, is to treat it with reverse osmosis, removing ions and generating clean water that can be recycled back into the feed tank where it is equilibrated with carbon dioxide to generate feed solution for the column. Sodium rejection as a function of water recovery for the XN-45 and Suez DK membrane is shown in Figure 12.

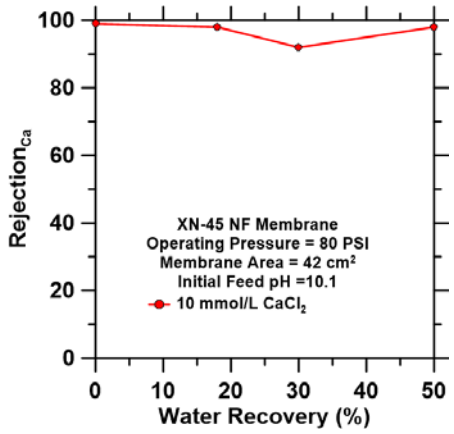
100
80
60
40
20
0
Rejection$_{Ca}$
XN-45 NF Membrane
Operating Pressure = 80 PSI
Membrane Area = 42 cm²
Initial Feed pH =10.1
10 mmol/L CaCl$_2$
0
10
20
30
40
50
Water Recovery (%)

(a)

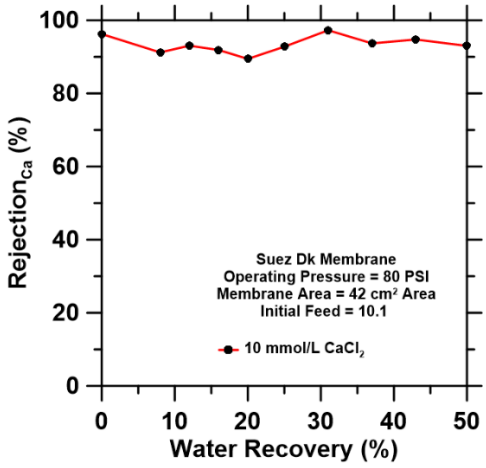
100
80
60
40
20
0
Rejection$_{Ca}$ (%)
Suez Dk Membrane
Operating Pressure = 80 PSI
Membrane Area = 42 cm² Area
Initial Feed = 10.1
10 mmol/L CaCl$_2$
0
10
20
30
40
50
Water Recovery (%)

(b)

Figure 12. (a) Sodium rejection as a function of water recovery for the XN-45 membrane, and **(b)** sodium rejection as a function of water recovery for the Suez DK membrane.

An ideal rejection would be 99% calcium with less than 10% sodium rejection. The Suez DK membrane has a rejection of roughly 85-90% calcium with a sodium rejection of 30%, not suitable for the Ion Exchange Process. The calcium rejection achieved with the XN-45 membrane was higher than 95% with ICP data confirming that the sodium rejection was within 10-15%. An important parameter in the process is permeate flux, the flow rate of the permeate from the nanofiltration cell. If the IEX process was to run continuously, the permeate flux would have to be high enough so that it does not impede the flows of the system. Permeate flux is shown in Figure 13 for the XN-45 and Suez DK membranes.

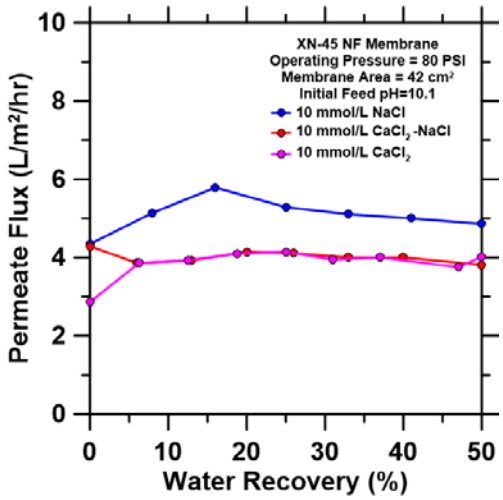
XN-45 NF Membrane
Operating Pressure = 80 PSI
Membrane Area = 42 cm²
Initial Feed pH=10.1
10 mmol/L NaCl
10 mmol/L CaCl2 -NaCl
10 mmol/L CaCl2
Permeate Flux (L/m²/hr)
Water Recovery (%)
0
2
4
6
8
10
0
10
20
30
40
50

(a)

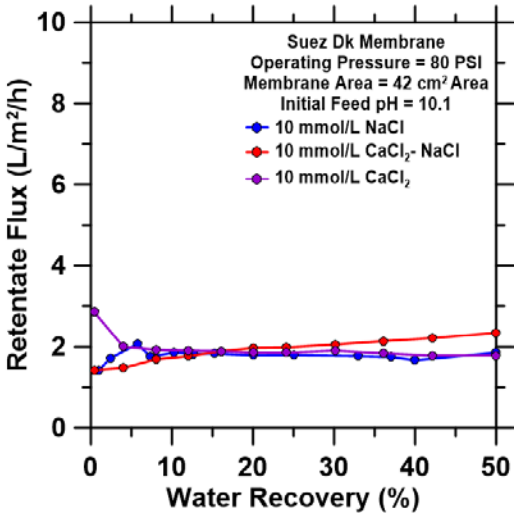
Suez Dk Membrane
Operating Pressure = 80 PSI
Membrane Area = 42 cm² Area
Initial Feed pH = 10.1
10 mmol/L NaCl
10 mmol/L CaCl2- NaCl
10 mmol/L CaCl2
Retentate Flux (L/m²/h)
Water Recovery (%)
0
2
4
6
8
10
0
10
20
30
40
50

(b)

Figure 13. (a) Permeate flux as a function of water recovery for the XN-45 membrane using single and mixed salts, and **(b)** permeate flux as a function of water recovery for the Suez DK membrane using single and mixed salts.

As shown in Figure 13a, permeate flux observed with the XN-45 membrane is noticeably higher for all salt conditions, single and mixed, at the same operating pressure than the Suez DK membrane as seen in Figure 13b. The increase in the permeate flux in Figure 13a can be attributed to an increase in temperature in the feed solution. As the temperature increases, membrane permeation increases due to the reduction in the solution's viscosity in addition to the increase of the diffusion phenomena through the membrane[57]. The permeate flux of both membranes could be improved by operating at a higher pressure, due to the larger gradient between the osmotic and applied pressures. However, even if permeate flux of the Suez DK can be increased, the calcium and sodium rejection is not sufficient enough for use in the Ion Exchange Process. The XN-45 membrane can be used to create a calcium rich retentate stream that can further be filtered with reverse osmosis to generate clean water that can be used for the feed and sodium rich permeate stream that can be used for regeneration of the ion exchange resin.

4 Conclusion

Our initial discovery is that the ion exchange process can induce alkalinity through the system to the degree that not only is precipitation favorable, but the system is also capable of handling high volumes of produced water without the need for consumable inorganic bases to achieve alkalinity. Pilot scale H^+ saturation capacities were constant at varying flow rates and at various regeneration conditions. For all cycles, during the regeneration of resin, stronger alkaline solutions (e.g., larger inlet OH^- concentrations) cause faster regeneration times to occur, due to the larger concentration gradient and acidic solutions exhaust the resin faster due to the higher proton concentration in solution. Precipitated solids were measured to be >97% calcite with magnesium and iron incorporation, dependent on the volume ratio used. The energy intensities associated with operating the pilot at a range of volume ratios was similar, between 40 – 62 kWh/t-CO_2 utilized for pCO_2 = 0.12 atm. The life cycle assessment demonstrates this process to be carbon-negative for partial pressures of CO_2 larger than 0.03 atm and for more concentrated produced water streams (-0.06 to -0.039 kg CO_2e per kg precipitated calcium carbonate). Nanofiltration studies confirm that the XN-45 membrane can be used to generate a sodium rich permeate stream and a calcium rich retentate stream that can be reused in the system.

APPENDIX

Supplementary information for the thesis

Pilot Plant Demonstration of Ion Exchange Process for Carbon Dioxide Mineralization Using Synthetic and Industrial Waste Streams

Summary

Data used in calculations

Table S1: Standard thermodynamic properties of minerals relating to the mineralization of CO_2 in divalent and alkaline rich systems at 25 °C and 1 bar. Data taken from Cemdata18 database [5] and other sources referenced in the table.

Minerals	Chemical formula	V°	$\Delta_f G^\circ_{298}$	$\Delta_f H^\circ_{298}$	S°_{298}	Cp°_{298}	Ref.
		($cm^3 \cdot mol^{-1}$)	($kJ \cdot mol^{-1}$)	($kJ \cdot mol^{-1}$)	($J \cdot mol^{-1}$)	($J \cdot mol^{-1} \cdot K^{-1}$)	
Aragonite	$CaCO_3$	34.2	-1207	-1128	90.2	81.3	[6,7]
Brucite	$Mg(OH)_2$	24.6	-923.0	-832.0	63.1	77.3	[6–8]
Dolomite	$CaMg(CO_3)_2$	64.4	-2157	-2317	166.7	157.7	[6,7]
Goethite	FeO(OH)	20.8	-497.3	-568.2	59.7	74.3	[9]
Hydromagnesite	$Mg_5(CO_3)_4(OH)_2(H_2O)_4$	21.1	-5836	-6516	520.0	571.1	[10]
Monohydrocalcite	$CaCO_3(H_2O)$	48.7	-1362	-1498	131.1	33.5	[9]
Nesquehonite	$MgCO_3(H_2O)_3$	75.5	-1726	-1977	75.5	195.6	[9]
Portlandite	$Ca(OH)_2$	33.1	-897.0	-984.7	83.4	87.5	[5]
$(Fe,Ca)CO_3$-ss*	$(Fe,Ca)CO_3$						[11]

Calcite	$CaCO_3$	36.9	-1207	-1129	92.7	81.90	[6,7]
Siderite	$FeCO_3$	29.4	-681.7	-751.9	105.0	82.09	[5]

Precipitation simulations using thermodynamic modeling

* Guggenheim parameters for non-ideal solid-solution model: $a_0 = 3.461$ and $a_1 = -0.551$

Table S2: Standard thermodynamic of aqueous species at 25 °C and 1 bar. Data taken from Cemdata18 database [5].

Species/complex	V°	$\Delta_f G^\circ_{298}$	$\Delta_f H^\circ_{298}$	S°_{298}	Cp°_{298}	Ref.
	($cm^3 \cdot mol^{-1}$)	($kJ \cdot mol^{-1}$)	($kJ \cdot mol^{-1}$)	($J \cdot mol^{-1}$)	($J \cdot mol^{-1} \cdot K^{-1}$)	
Ca^{2+}	-18.4	-543.1	-552.8	-56.5	-30.9	[12]
$CaOH^+$	5.8	-751.6	-717.0	28.0	6.0	[12]
$CaSO_4^o$	4.7	-1448	-1310	20.9	-104.6	[13]
$CaCO_3^o$	-1.6	-1202	-1099	10.5	-123.9	[13]
$CaHCO_3^+$	13.3	-1232	-1146	66.9	233.7	[6,7]
Fe^{2+}	-2.26	-91.5	-92.24	-105.8	-32.4	[2,8]
$FeCO_3$	-1.72	-644.4	-763.5	-58.45	-123.0	[2,8]
$FeHCO_3^+$	0.818	-689.8	-794.0	-8.87	231.4	[2,8]
$FeHSO_4^+$	1.88	-853.4	-990.4	10.2	338.2	[2,8]
$FeSO_4$	0.167	-848.8	-993.8	-16.8	-101.6	[2,8]
$FeCl^+$	0.0845	-223.5	-258.0	-42.0	86.5	[6,6,13]
$FeOH^+$	-1.671	-274.4	-325.6	-41.8	63.1	[6,6,13]
Fe^{3+}	-3.77	-17.1	-49.5	-277.3	-76.7	[2,8]
$FeHSO_4^{2+}$	0.231	-787.1	-981.9	-248.9	426.7	[2,8]
$FeSO_4^+$	-0.263	-784.7	-942.4	-124.6	-145.9	[2,8]
$Fe(SO_4)^{2-}$	3.04	-1536.8	-1854.3	-87.7	-210.3	[2,8]
$FeCl_2^+$	-2.28	-156.9	-212.6	-178.8	14.8	[2,8]
$FeCl^{2+}$	1.02	-291.9	-385.7	-129.6	300.7	[2,8]
$FeCl_3$	3.59	-417.5	-564.3	-131.0	368.2	[2,8]
FeO^+	-4.20	-222.0	-255.0	-46.4	-200.9	[2,8]
FeO_2^-	0.0451	-368.2	-443.8	44.3	-234.9	[2,8]
FeO_2H	0.720	-419.8	-480.9	92.8	-312.1	[2,8]

$FeOH^{2+}$	-2.53	-241.8	-292.7	-106.2	-33.7	[2,8]
K^+	9.0	-282.5	-252.1	101.0	8.4	[12]
KOH^o	15.0	-437.1	-474.1	108.4	-85.0	[12]
KSO_4^{2-}	27.5	0.0	-1031.8	146.4	-45.1	[12,13]
Na^+	-1.2	-240.3	-261.9	58.4	38.1	[12]
$NaOH^o$	3.5	-470.1	-418.1	44.8	-13.4	[12]
$NaSO_4^-$	18.6	-1147	-1010	101.8	-30.1	[14]
$NaCO_3^-$	-0.4	-938.6	-797.1	-44.3	-51.3	[6,7]
$NaHCO_3^o$	32.3	-929.5	-847.4	154.7	200.3	[6,7]
HSO_3^-	33.0	-627.7	-529.1	139.7	-5.4	[12]
SO_3^{2-}	-4.1	-636.9	-487.9	-29.3	-281.0	[12]
HSO_4^-	34.8	-889.2	-755.8	125.5	22.7	[12]
SO_4^{2-}	12.9	-909.7	-744.5	18.8	-266.1	[12]
H_2S^o	35.0	-39.0	-27.9	125.5	179.2	[12]
HS^-	20.2	-16.2	12.0	68.2	-93.9	[12]
S^{2-}	20.2	92.2	120.4	68.2	-93.9	[12]
Mg^{2+}	-22.0	-465.9	-454.0	-138.1	-21.7	[12]
$MgOH^+$	1.6	-690.0	-625.9	-79.9	129.2	[12]
$MgCO_3^o$	-16.7	-1132	-999.0	-100.4	-116.5	[6,7,13]
$MgHCO_3^+$	9.3	-1154	-1047	-12.6	254.4	[6,7]
CO_2^o	32.8	-413.8	-386.0	117.6	243.1	[6,7,15]
CO_3^{2-}	-6.1	-675.3	-528.0	-50.0	-289.3	[12]
HCO_3^-	24.2	-690.0	-586.9	98.5	-34.8	[12]
OH^-	-4.7	-230	-157.3	-10.7	-136.3	[12]
H^+	0	0	0	0	0	[12]
H_2O^o	18.1	-285.9	-237.2	69.9	75.4	[16]
H_2^o	25.3	-4.0	17.7	57.7	166.9	[6,7,15]
N_2^o	33.4	-10.4	18.2	95.8	234.2	[15]
O_2^o	30.5	-12.2	16.4	109	234.1	[15]

[o] denotes neutral species within aqueous solution.

Table S3: Thermodynamic properties of the gases used in the thermodynamic simulations.

Gases*	V°	$\Delta_f G^\circ_{298}$	$\Delta_f H^\circ_{298}$	S°_{298}	Cp°_{298}	Ref.
	($cm^3 \cdot mol^{-1}$)	(kJ·mol^{-1})	(kJ·mol^{-1})	(J·mol^{-1})	(J·mol^{-1}·K^{-1})	
N_2	24790	0	0	191.6	29.1	[17]
O_2	24790	0	0	205.1	29.3	[17]
H_2	24790	0	0	130.7	28.8	[17]
CO_2	24790	-393.5	-394.4	213.7	37.1	[17]
CH_4	24790	-74.8	-50.7	186.2	35.7	[17]
H_2S	24790	-20.6	-33.8	205.8	34.2	[17]

*H_2O (g) was omitted from the thermodynamic modelling simulations. Omitting this gaseous phase provides a greater stability of the aqueous phase within the modelling results.

Results and Discussion section supplementary material

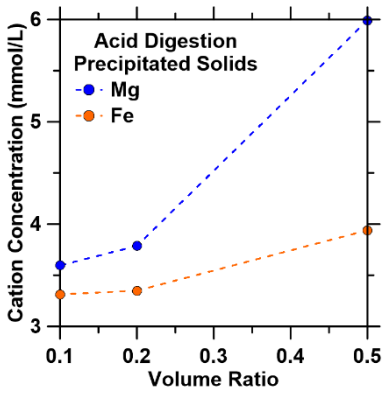

Figure S1. Acid digestion of precipitated solids at varying volume ratios.

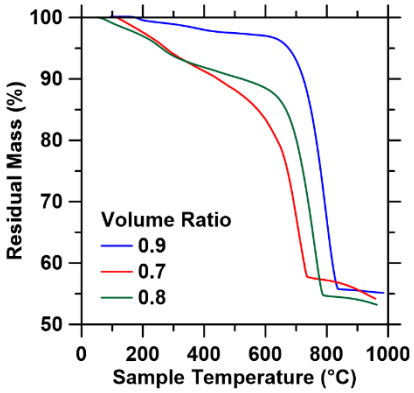

Figure S2. Thermogravimetric analysis of precipitated calcium carbonate solids at varying volume ratios.

References

(1) US EPA, O. *Inventory of U.S. Greenhouse Gas Emissions and Sinks*. https://www.epa.gov/ghgemissions/inventory-us-greenhouse-gas-emissions-and-sinks (accessed 2023-05-24).

(2) *Global CO2 emissions from energy combustion and industrial processes, 1900-2022 – Charts – Data & Statistics*. IEA. https://www.iea.org/data-and-statistics/charts/global-co2-emissions-from-energy-combustion-and-industrial-processes-1900-2022 (accessed 2023-05-24).

(3) *CO2 Emissions in 2022 – Analysis*. IEA. https://www.iea.org/reports/co2-emissions-in-2022 (accessed 2023-05-24).

(4) US EPA, O. *Sources of Greenhouse Gas Emissions*. https://www.epa.gov/ghgemissions/sources-greenhouse-gas-emissions (accessed 2023-05-24).

(5) Stewart, D. R.; Stewart, A. D. R.; Guthrie, R. F. Utilizing Produced Water as a New Water Resource.

(6) Zemlick, K.; Kalhor, E.; Thomson, B. M.; Chermak, J. M.; Sullivan Graham, E. J.; Tidwell, V. C. Mapping the Energy Footprint of Produced Water Management in New Mexico. *Environ. Res. Lett.* **2018**, *13* (2), 024008. https://doi.org/10.1088/1748-9326/aa9e54.

(7) Pan, S.-Y.; Chen, Y.-H.; Fan, L.-S.; Kim, H.; Gao, X.; Ling, T.-C.; Chiang, P.-C.; Pei, S.-L.; Gu, G. CO2 Mineralization and Utilization by Alkaline Solid Wastes for Potential Carbon Reduction. *Nat Sustain* **2020**, *3* (5), 399–405. https://doi.org/10.1038/s41893-020-0486-9.

(8) Huijgen, W. J. J.; Comans, R. N. J.; Witkamp, G.-J. Cost Evaluation of CO2 Sequestration by Aqueous Mineral Carbonation. *Energy Conversion and Management* **2007**, *48* (7), 1923–1935. https://doi.org/10.1016/j.enconman.2007.01.035.

(9) Hills, C. D.; Tripathi, N.; Carey, P. J. Mineralization Technology for Carbon Capture, Utilization, and Storage. *Frontiers in Energy Research* **2020**, *8*.

(10) El Hadri, N.; Quang, D. V.; Goetheer, E. L. V.; Abu Zahra, M. R. M. Aqueous Amine Solution Characterization for Post-Combustion CO2 Capture Process. *Applied Energy* **2017**, *185*, 1433–1449. https://doi.org/10.1016/j.apenergy.2016.03.043.

(11) Kim, S.; Shi, H.; Lee, J. Y. CO2 Absorption Mechanism in Amine Solvents and Enhancement of CO2 Capture Capability in Blended Amine Solvent. *International Journal of Greenhouse Gas Control* **2016**, *45*, 181–188. https://doi.org/10.1016/j.ijggc.2015.12.024.

(12) Wang, X.; Song, C. Carbon Capture From Flue Gas and the Atmosphere: A Perspective. *Frontiers in Energy Research* **2020**, *8*.

(13) Chai, S. Y. W.; Ngu, L. H.; How, B. S. Review of Carbon Capture Absorbents for CO2 Utilization. *Greenhouse Gases: Science and Technology* **2022**, *12* (3), 394–427. https://doi.org/10.1002/ghg.2151.

(14) Eide, L. I.; Batum, M.; Dixon, T.; Elamin, Z.; Graue, A.; Hagen, S.; Hovorka, S.; Nazarian, B.; Nøkleby, P. H.; Olsen, G. I.; Ringrose, P.; Vieira, R. A. M. Enabling Large-Scale Carbon Capture, Utilisation, and Storage (CCUS) Using Offshore Carbon Dioxide (CO2) Infrastructure Developments—A Review. *Energies* **2019**, *12* (10), 1945. https://doi.org/10.3390/en12101945.

(15) *U.S. Geological Survey National Produced Waters Geochemical Database v2.3 | USGS Science Data Catalog*.

https://data.usgs.gov/datacatalog/data/USGS:59d25d63e4b05fe04cc235f9 (accessed 2022-06-14).

(16) King, D. W.; Farlow, R. Role of Carbonate Speciation on the Oxidation of Fe(II) by H2O2. *Marine Chemistry* **2000**, *70* (1), 201–209. https://doi.org/10.1016/S0304-4203(00)00026-8.

(17) Kumar, A.; Du, F.; Lienhard, J. H. V. Caustic Soda Production, Energy Efficiency, and Electrolyzers. *ACS Energy Lett.* **2021**, *6* (10), 3563–3566. https://doi.org/10.1021/acsenergylett.1c01827.

(18) Bustillos, S.; Alturki, A.; Prentice, D.; La Plante, E. C.; Rogers, M.; Keller, M.; Ragipani, R.; Wang, B.; Sant, G.; Simonetti, D. A. Implementation of Ion Exchange Processes for Carbon Dioxide Mineralization Using Industrial Waste Streams. *Frontiers in Energy Research* **2020**, *8*.

(19) Bustillos, S.; Prentice, D.; La Plante, E. C.; Wang, B.; Sant, G.; Simonetti, D. Process Simulations Reveal the Carbon Dioxide Removal Potential of a Process That Mineralizes Industrial Waste Streams via an Ion Exchange-Based Regenerable PH Swing. *ACS Sustainable Chem. Eng.* **2022**, *10* (19), 6255–6264. https://doi.org/10.1021/acssuschemeng.2c00458.

(20) *The hydration of carbon dioxide* | *Journal of Chemical Education*. https://pubs.acs.org/doi/10.1021/ed037p14 (accessed 2023-05-24).

(21) Robin, V.; Tertre, E.; Beaufort, D.; Regnault, O.; Sardini, P.; Descostes, M. Ion Exchange Reactions of Major Inorganic Cations (H+, Na+, Ca2+, Mg2+ and K+) on Beidellite: Experimental Results and New Thermodynamic Database. Toward a Better Prediction of Contaminant Mobility in Natural Environments. *Applied Geochemistry* **2015**, *59*, 74–84. https://doi.org/10.1016/j.apgeochem.2015.03.016.

(22) Avena, M. J.; De Pauli, C. P. Proton Adsorption and Electrokinetics of an Argentinean Montmorillonite. *Journal of Colloid and Interface Science* **1998**, *202* (1), 195–204. https://doi.org/10.1006/jcis.1998.5402.

(23) Tasker, T. L.; Warner, N. R.; Burgos, W. D. Geochemical and Isotope Analysis of Produced Water from the Utica/Point Pleasant Shale, Appalachian Basin. *Environ. Sci.: Processes Impacts* **2020**, *22* (5), 1224–1232. https://doi.org/10.1039/D0EM00066C.

(24) Kulik, D. A.; Wagner, T.; Dmytrieva, S. V.; Kosakowski, G.; Hingerl, F. F.; Chudnenko, K. V.; Berner, U. R. GEM-Selektor Geochemical Modeling Package: Revised Algorithm and GEMS3K Numerical Kernel for Coupled Simulation Codes. *Comput Geosci* **2012**. https://doi.org/10.1007/s10596-012-9310-6.

(25) Wagner, T.; Kulik, D. A.; Hingerl, F. F.; Dmytrieva, S. V. GEM-SELEKTOR GEOCHEMICAL MODELING PACKAGE: TSolMod LIBRARY AND DATA INTERFACE FOR MULTICOMPONENT PHASE MODELS. *The Canadian Mineralogist* **2012**, *50* (5), 1173–1195. https://doi.org/10.3749/canmin.50.5.1173.

(26) Hummel, W.; Berner, U.; Curti, E.; Pearson, F.; Thoenen, T. Nagra/PSI Chemical Thermodynamic Data Base 01/01. **2002**. https://doi.org/10.1524/ract.2002.90.9-11_2002.805.

(27) Thoenen, T.; Hummel, W.; Berner, U.; Curti, E. *The PSI/Nagra Chemical Thermodynamic Database 12/07*; Villigen PSI; Paul Scherrer Institut: Switzerland, 2007.

(28) Lothenbach, B.; Kulik, D. A.; Matschei, T.; Balonis, M.; Baquerizo, L.; Dilnesa, B.; Miron, G. D.; Myers, R. J. Cemdata18: A Chemical Thermodynamic Database for Hydrated Portland Cements and Alkali-Activated Materials. *Cement and Concrete Research* **2019**, *115*, 472–506. https://doi.org/10.1016/j.cemconres.2018.04.018.

(29) Johnson, J. W.; Oelkers, E. H.; Helgeson, H. C. SUPCRT92: A Software Package for Calculating the Standard Molal Thermodynamic Properties of Minerals, Gases, Aqueous Species, and Reactions from 1 to 5000 Bar and 0 to 1000°C. *Computers & Geosciences* **1992**, *18* (7), 899–947. https://doi.org/10.1016/0098-3004(92)90029-Q.

(30) Robie, R.; Hemingway, B. *Thermodynamic Properties of Minerals and Related Substances at 298.15 K and 1 Bar (105 Pascals) Pressure and at Higher Temperatures*; U.S Geological Survey Bulletin; 2131; 1995.

(31) Galvez-Martos, J.-L.; Elhoweris, A.; Morrison, J.; Al-horr, Y. Conceptual Design of a CO2 Capture and Utilisation Process Based on Calcium and Magnesium Rich Brines. *Journal of CO2 Utilization* **2018**, *27*, 161–169. https://doi.org/10.1016/j.jcou.2018.07.011.

(32) Di Lorenzo, F.; Burgos-Cara, A.; Ruiz-Agudo, E.; Putnis, C. V.; Prieto, M. Effect of Ferrous Iron on the Nucleation and Growth of $CaCO_3$ in Slightly Basic Aqueous Solutions. *CrystEngComm* **2017**, *19* (3), 447–460. https://doi.org/10.1039/C6CE02290A.

(33) Helgeson, H. C.; Kirkham, D. H.; Flowers, G. C. Theoretical Prediction of the Thermodynamic Behavior of Aqueous Electrolytes by High Pressures and Temperatures; IV, Calculation of Activity Coefficients, Osmotic Coefficients, and Apparent Molal and Standard and Relative Partial Molal Properties to 600 Degrees C and 5kb. *Am J Sci* **1981**, *281* (10), 1249–1516. https://doi.org/10.2475/ajs.281.10.1249.

(34) *Hydraulic Power - an overview | ScienceDirect Topics*. https://www.sciencedirect.com/topics/engineering/hydraulic-power (accessed 2023-06-12).

(35) *Mixing Power - an overview | ScienceDirect Topics*. https://www.sciencedirect.com/topics/engineering/mixing-power (accessed 2023-06-12).

(36) 14:00-17:00. *ISO 14040:2006*. ISO. https://www.iso.org/standard/37456.html (accessed 2023-06-12).

(37) 14:00-17:00. *ISO 14044:2006*. ISO. https://www.iso.org/standard/38498.html (accessed 2023-06-12).

(38) Mattila, H.-P.; Hudd, H.; Zevenhoven, R. Cradle-to-Gate Life Cycle Assessment of Precipitated Calcium Carbonate Production from Steel Converter Slag. *Journal of Cleaner Production* **2014**, *84*, 611–618. https://doi.org/10.1016/j.jclepro.2014.05.064.

(39) Batuecas, E.; Liendo, F.; Tommasi, T.; Bensaid, S.; Deorsola, F. A.; Fino, D. Recycling CO2 from Flue Gas for CaCO3 Nanoparticles Production as Cement Filler: A Life Cycle Assessment. *Journal of CO2 Utilization* **2021**, *45*, 101446. https://doi.org/10.1016/j.jcou.2021.101446.

(40) Alrehaili, O.; Perreault, F.; Sinha, S.; Westerhoff, P. Increasing Net Water Recovery of Reverse Osmosis with Membrane Distillation Using Natural Thermal Differentials between Brine and Co-Located Water Sources: Impacts at Large Reclamation Facilities. *Water Research* **2020**, *184*, 116134. https://doi.org/10.1016/j.watres.2020.116134.

(41) Boo, C.; Wang, Y.; Zucker, I.; Choo, Y.; Osuji, C. O.; Elimelech, M. High Performance Nanofiltration Membrane for Effective Removal of Perfluoroalkyl Substances at High Water Recovery. *Environ. Sci. Technol.* **2018**, *52* (13), 7279–7288. https://doi.org/10.1021/acs.est.8b01040.

(42) Nauman, E. B. Residence Time Theory. *Ind. Eng. Chem. Res.* **2008**, *47* (10), 3752–3766. https://doi.org/10.1021/ie071635a.

(43) Borba, C. E.; Guirardello, R.; Silva, E. A.; Veit, M. T.; Tavares, C. R. G. Removal of Nickel(II) Ions from Aqueous Solution by Biosorption in a Fixed Bed Column: Experimental

and Theoretical Breakthrough Curves. *Biochemical Engineering Journal* **2006**, *30* (2), 184–191. https://doi.org/10.1016/j.bej.2006.04.001.

(44) Chatterjee, S.; Mondal, S.; De, S. Design and Scaling up of Fixed Bed Adsorption Columns for Lead Removal by Treated Laterite. *Journal of Cleaner Production* **2018**, *177*, 760–774. https://doi.org/10.1016/j.jclepro.2017.12.249.

(45) Barros, M. A. S. D.; Silva, E. A.; Arroyo, P. A.; Tavares, C. R. G.; Schneider, R. M.; Suszek, M.; Sousa-Aguiar, E. F. Removal of Cr(III) in the Fixed Bed Column and Batch Reactors Using as Adsorbent Zeolite NaX. *Chemical Engineering Science* **2004**, *59* (24), 5959–5966. https://doi.org/10.1016/j.ces.2004.07.040.

(46) Kang, S.-Y.; Lee, J.-U.; Moon, S.-H.; Kim, K.-W. Competitive Adsorption Characteristics of Co2+, Ni2+, and Cr3+ by IRN-77 Cation Exchange Resin in Synthesized Wastewater. *Chemosphere* **2004**, *56* (2), 141–147. https://doi.org/10.1016/j.chemosphere.2004.02.004.

(47) Lee, S.-K.; Lee, U.-H. Adsorption and Desorption Property of Iminodiacetate Resin (Lewatit® TP207) for Indium Recovery. *Journal of Industrial and Engineering Chemistry* **2016**, *40*, 23–25. https://doi.org/10.1016/j.jiec.2016.05.016.

(48) Pessu, F.; Barker, R.; Neville, A. The Influence of PH on Localized Corrosion Behavior of X65 (UNS K03014) Carbon Steel in CO2-Saturated Brines. *Corrosion* **2015**, *2015*. https://doi.org/10.5006/1770.

(49) Mucci, A.; Morse, J. W. The Incorporation of Mg2+ and Sr2+ into Calcite Overgrowths: Influences of Growth Rate and Solution Composition. *Geochimica et Cosmochimica Acta* **1983**, *47* (2), 217–233. https://doi.org/10.1016/0016-7037(83)90135-7.

(50) Dromgoole, E. L.; Walter, L. M. Iron and Manganese Incorporation into Calcite: Effects of Growth Kinetics, Temperature and Solution Chemistry. *Chemical Geology* **1990**, *81* (4), 311–336. https://doi.org/10.1016/0009-2541(90)90053-A.

(51) *Enhanced Crystallographic Incorporation of Strontium(II) Ions into Calcite via Preferential Adsorption at Obtuse Growth Steps | Crystal Growth & Design*. https://pubs.acs.org/doi/10.1021/acs.cgd.7b01614 (accessed 2023-06-12).

(52) Xto, J. M.; Du, H.; Borca, C. N.; Amstad, E.; van Bokhoven, J. A.; Huthwelker, T. Tuning the Incorporation of Magnesium into Calcite during Its Crystallization from Additive-Free Aqueous Solution. *Crystal Growth & Design* **2019**, *19* (8), 4385–4394. https://doi.org/10.1021/acs.cgd.9b00179.

(53) Xiao-Fei, Q.; Yao, Q.-Z.; Zhou, G.-T. Synthesis of Siderite Microspheres and Their Transformation to Magnetite Microspheres. *European Journal of Mineralogy* **2011**, *23*, 757–770. https://doi.org/10.1127/0935-1221/2011/0023-2134.

(54) *U.S. energy facts explained - consumption and production - U.S. Energy Information Administration (EIA)*. https://www.eia.gov/energyexplained/us-energy-facts/ (accessed 2023-06-14).

(55) Stewart, D. R.; Stewart, A. D. R.; Guthrie, R. F. Utilizing Produced Water as a New Water Resource.

(56) Chu, C.-H.; Wang, C.; Xiao, H.-F.; Wang, Q.; Yang, W.-J.; Liu, N.; Ju, X.; Xie, J.-X.; Sun, S.-P. Separation of Ions with Equivalent and Similar Molecular Weights by Nanofiltration: Sodium Chloride and Sodium Acetate as an Example. *Separation and Purification Technology* **2020**, *250*, 117199. https://doi.org/10.1016/j.seppur.2020.117199.

(57) Shigidi, I.; Anqi, A. E.; Elkhaleefa, A.; Mohamed, A.; Ali, I. H.; Brima, E. I. Temperature Impact on Reverse Osmosis Permeate Flux in the Remediation of Hexavalent Chromium. *Water* **2022**, *14* (1), 44. https://doi.org/10.3390/w14010044.